Chin. J. Astron. Astrophys. Vol. 8 (2008), No. 2, 179–194
(*http://www.chjaa.org*)

Chinese Journal of
Astronomy and
Astrophysics

Bending of Jets in the QSO NRAO 530 *

Xiao-Yu Hong[1], Chuan-Hao Sun[1,2], Jun-Hui Zhao[3], Dong-Rong Jiang[1], Zhi-Qiang Shen[1,4], Tao An[1], Wei-Hua Wang[1] and Jun Yang[1,2]

[1] Shanghai Astronomical Observatory, Chinese Academy of Sciences, Shanghai 200030; *xhong@shao.ac.cn*
[2] Graduate University of Chinese Academy of Sciences, Beijing 100049
[3] Harvard-Smithsonian Center for Astrophysics, 60 Garden street, MS 72, Cambridge, MA02138
[4] Joint Institute for Galaxy and Cosmology

Received 2007 July 3; accepted 2007 August 8

Abstract We present radio images of NRAO 530 on scales ranging from pc to kpc. The observations include the EVN at 5 GHz, the VLBA at 1.6, 8.6 and 15 GHz, the MERLIN at 1.6 and 5 GHz, and the VLA at 5, 8.4, 15, 22, and 43 GHz. The VLBI images show a core-jet structure with an oscillating trajectory on a scale of about 30 mas north of the strongest compact component (core). Superluminal motions are detected in five of the jet components with apparent velocities in the range of 13.6 to 25.2c. A new component is detected at 15 GHz with the VLBA observations, which appears to be associated with the outburst in 2002. Significant polarized emission is detected around the core with the VLBA observations at 15 GHz. Rapid variations of the polarization intensity and angle are found between the epochs in 2002 and 2004. On the kpc-scale, a distant component (labelled as WL) located 11 arcsec west (PA=$-86°$) of the core is detected beyond the core-jet structure which extended to several hundreds of mas in the north-west direction ($-50\,°$). A significant emission between the core-jet structure and the WL is revealed. A clump of diffuse emission (labelled EL, 12 arcsec long) at PA $70°$ to the core, is also detected in the VLA observations, suggesting the presence of double lobes in the source. The core component shows a flat spectrum, while the distant components WL and EL have steep spectra. The steep spectra of the distant components and the detection of the arched emission suggest that the distant components are lobes or hot-spots powered by the core of NRAO 530. The morphologies from pc- to kpc-scales and the bending of jets are investigated. The observed radio morphology from pc to kcp appears to favor the model in which precession or wobbling of the nuclear disk drives the helical motion of the radio plasma and produces the S-shaped structure on kpc scale.

Key words: galaxies: nuclei — galaxies: jets — quasars: individual: NRAO 530

1 INTRODUCTION

The quasar, NRAO 530 (also 1730–130), is a well known optically violently variable (OVV) extragalactic source with $m_{\rm pg} \sim 18.5$ mag (Whelch & Spinrad 1973) at a redshift of 0.902 (Junkkarinen 1984). This source has been observed at almost all wavelengths from radio to γ-ray. Weak polarization of the source was detected in both the optical and radio bands. NRAO 530 was identified as a γ-ray source by the Energetic Gamma Ray Experiment Telescope (EGRET) with a flux density of 4.6×10^{-11} Jy at 2.55 GeV (Fichtel et al. 1994; Thompson et al. 1995). This source was also detected by the Röntgen Satellite ($ROSAT$) with 1.84×10^{-6} Jy at 1.3 keV (Brinkmann et al. 1994).

∗ Supported by the National Natural Science Foundation of China.

NRAO 530 was extensively monitored as a low-frequency variable source (e.g., Bondi et al. 1994). Three-epoch early VLBI (Very Long Baseline Interferometry) observations at 1.7 GHz showed a structure oriented in the north-south direction extending 25 milli-arcsec (mas) at PA$= -7^\circ$ (Romney et al. 1984; Bondi et al. 1994). Two-epoch VLBI observations at 5 GHz showed a 4-mas slightly curved jet towards the north direction, and no counter jet has been detected (Shen et al. 1997; Hong et al. 1999). A jet-like feature extended approximately 5 mas from the core along PA$\sim 15^\circ$ can be observed with the VLBI at 8.5 GHz (Tingay et al. 1998).

The source underwent a dramatic radio outburst in 1995 with a flux density higher than any value observed over 30 years of monitoring (Bower et al. 1997). The creation of new components in the jet associated with the outbursts was revealed by their 86 GHz VLBI observation with one component (C1, in their notation) to a radio outburst observed in mid 1994 and another component (C2) to the 1995 outburst. The components move to the south-west with apparent velocities of 10.4 and 11.1c, respectively, by assuming the brightest component as the core (Bower et al. 1997).

Monitoring of the source at 22 and 43 GHz VLBA was made during the flare in 1995 (five epochs from 1994.45 to 1996.90) by Jorstad et al. (2001). Based on the data with a better time-sampling, the authors interpreted the evolution by assuming the south-end component as the core and the brightness feature as the ejected component during the flare. Their results showed that the structure is extended to north and the motion of the component is roughly towards north with apparent velocities in the range of 9.8 to 40.8c, while there was a stationary feature located at a distance $\sim$1.4 mas north of the core (Jorstad et al. 2001).

NRAO530 was monitored at 15 GHz as one of 133 AGNs in the MOJAVE program (Monitoring of Jets in AGN with VLBA Experiments) by Lister et al. (2005). This program with a better sample is not only good for statistic analysis, but also good for individual source studies.

Feng et al. (2006) studied the source with multiple-frequency (5, 8, 22, 39, 43 and 45 GHz) VLBA observations. It shows a core-dominated morphology with a bending jet to the north of the core. Superluminal speeds of 10.2c and 14.5c were detected from the two jet components.

VLA observation of the source at 1.6 GHz showed an unresolved core and a second unresolved component $11''$ distant at PA -90° (Perley 1982) with no evidence for a connection between the two sources (Romney et al. 1984).

The detection of the source indicates that evidence for relativistic bulk motion of the emitting plasma exists in its nucleus. A Doppler factor of 5.2 of NRAO 530 was estimated on assuming equipartition between the energy of the particles and magnetic field (Güijosa & Daly 1996).

In this paper, we investigate the structure variation at pc-scale and the extended radio emission of the source at kpc-scale with the VLBA, the EVN, the MERLIN, and the VLA observations at multi-frequencies of 1.6, 5, 8, 15, 22 and 43 GHz.

The cosmological parameters are taken to be Ω_M=0.3, Ω_Λ=0.7 (Riess 2004), $H_0 = 73$ km s^{-1} Mpc^{-1} (Riess 2005) throughout this paper. For NRAO 530 at redshift 0.902, 1 mas angular size corresponds to 7.8 pc.

2 OBSERVATIONS

We observed NRAO 530 with numerous interferometer arrays. We also searched and re-analyzed the archived data of this source. The setup of the observations used in this paper is summarized in the following.

2.1 EVN Observation

A full-track 7-hour EVN + MERLIN observation of the NRAO 530 was carried out at 5 GHz on 1999 February 19. The EVN consists of telescopes of Effelsberg, Shanghai, Cambridge, Jodrell Bank (Mark 2), Medicina, Noto, Onsala, Urumqi, WSRT and Torun. The data were recorded with the Mk III VLBI recording system in Mode B with an effective bandwidth of 28 MHz and correlated at the Max-Plank Institut für Radioastronomie in Bonn. The detailed information is listed in Table 1.

2.2 VLBA Observations

The three datasets of VLBA archive data at 15 GHz (MOJAVE program), which were kindly provided by M. Lister, were re-analyzed. The observations were carried out in a snap shot mode at the epochs of

Table 1 Epochs, Frequencies and Arrays of the Observations

No.[a]	Epoch	Freq.[b]	Bandwidth (MHz)	T[c] (min.)	Array	Ant[d]	Correlator	P.I. & Note
1	2000.03	U	60	35	VLBA	All 10	VLBA[e]	Kellerman et al.
2[f]	2002.77	U	128	60	VLBA	All 10	VLBA	Lister et al. 2005
3[f]	2004.12	U	128	60	VLBA	All 10	VLBA	Lister et al. 2005
4	1999.13	C	28	240	EVN	EVN(10)	MPIfR[g]	Hong et al.
5	1999.45	L	64	24	VLBA	All 10	VLBA	Fomalont, fringe finder
6	1999.13	C	14	240	MERLIN	6	MERLIN	Hong et al.
7	1998.35	L	14	120	MERLIN	All 7	MERLIN	S. Eyres, phase ref.
8	1992.91	X	50	13	VLA	All 27	VLA	Zhao et al., calibrator
9	2003.46	C	100	7	VLA	All 27	VLA	Zhao et al., calibrator
10[h]		U K Q	100	2-4	VLA-A	All 27	VLA	Zhao et al., calibrator
11[i]		U K Q	100	2-4	VLA-AnB	All 27	VLA	Zhao et al., calibrator
12[j]		U K Q	100	2-4	VLA-B	All 27	VLA	Zhao et al., calibrator
13[k]		U K Q	100	2-4	VLA-BnC	All 27	VLA	Zhao et al., calibrator
14[l]		U K Q	100	2-4	VLA-C	All 27	VLA	Zhao et al., calibrator
15	2003.04	U K Q	100	4	VLA-CnD	All 27	VLA	Zhao et al., calibrator
16[m]		U K Q	100	2-4	VLA-D	All 27	VLA	Zhao et al., calibrator

[a] With the order from high resolution array to the low resolution array
[b] Freq.: L: 1.6 GHz, C: 5 GHz, X: 8.4 GHz, U: 15 GHz, K:22 GHZ, Q:43 GHz
[c] On source time
[d] EVN(10): Effelsberg, Shanghai, Cambridge, Jodrell Bank (MK2), Medicina, Noto, Onsala, Urumqi,WSRT, Torun; MERLIN(6): Defford, Cambridge, Knockin, Darnhall, Mark 2, and Tabley; MERLIN(7)=MERLIN(6)+Lovell
[e] The NRAO VLBA correlator (Socorro, USA)
[f] Dual polarized observations
[g] The MK III correlator at MPIfR (Bonn, Germany)
[h] 13 epochs from 2002 Feb. 2, to 2002 May 5
[i] 3 epochs from 2002 May 20, to 2002 Jun. 7
[j] 11 epochs from 2002 Jun. 16, 2002 to Sep. 10
[k] 3 epochs from 2002 Sep. 18, to 2002 Oct. 3
[l] 7 epochs from 2002 Oct. 12, to 2003 Jan. 4
[m] 3 epochs from 2003 Feb. 14, to 2003 Apr. 16

2000.03, 2002.77 and 2004.12 with observing times of 35, 65 and 60 minutes, respectively. The data were recorded with a bandwidth of 60 MHz at the first epoch in right-handed circular polarization mode, and with a bandwidth of 128 MHz for the rest two in dual polarization mode. The raw data were correlated with the VLBA correlator in Socorro, NM, USA. The detailed information is listed in Table 1.

The archive data of VLBA at 1.6 GHz were analyzed. The observation was carried out at the epoch of 1999.45 with 24 minutes on source as a fringe finder and the rough data were recorded with a bandwidth of 64 MHz (see Table 1).

2.3 MERLIN Observations

The 5-GHz MERLIN observation was carried out on 1999 February 19 together with the EVN as described in Section 2.1. The MERLIN array consists of six antennas (Defford, Cambridge, Knockin, Darnhall, Mark 2 and Tabley). The central frequency was 4.994 MHz with a bandwidth of 14 MHz.

NRAO 530 was observed at 1.6 GHz as a phase reference source for a total of 2 hours on source including 46 scans over a time period of 8 hours (provided by S. T. Garrington). The observation was carried out on 1998 May 8. The array consists of seven antennas (the above-mentioned six plus Lovell). The bandwidth was 14 MHz (see Table 1). We imaged and model-fitted MERLIN data for our study in this paper.

2.4 VLA Observations

NRAO 530 was observed with the VLA on 1992 November 27 at 8.4 GHz and on 2003 June 17 at 4.8 GHz as a calibrator. The observations were carried out with a total bandwidth of 100 MHz.

Table 2 Parameters of the Images

Fig.	Epoch	Array	Band (GHz)	$S_{\rm peak}$ (Jy beam^{-1})	r.m.s. (mJy beam^{-1})	Contours (mJy beam^{-1})	Restoring Beam Maj×Min(mas), PA($^\circ$)	
(1)	(2)	(3)	(4)	(5)	(6)	(7)	(8)	
2a	2002.77	VLBA	15.0	4.74	0.18	$1.0\times(-1,1,2,4,...,1024)$	1.4×0.5,	-5.3
2b	1999.13	EVN	5.0	2.70	1.50	$5.0\times(-1,1,2,4,...,512)$	5.8×4.4,	46.6
2c	1999.45	VLBA	1.6	3.09	0.81	$2.5\times(-1,1,2,4,...,1024)$	4.6×11.7,	6.3
2d	1998.35	MERLIN	1.6	5.00	0.30	$1.0\times(-1,1,2,4,...,1024)$	440×250,	12.1
2e	2003.46	VLA-A	5.0	4.83	0.15	$0.40\times(-1,1,2,4,...,1024)$	790×430,	29.0
2f	2003.03	VLA-CnD	14.9	5.45	0.26	$0.80\times(-1,1,2,4,...,1024)$	3000×3000,	0
2g	2003.29	VLA-D	15.0	5.20	0.15	$0.25\times(-1,1,2,4,...,1024)$	6720×3860,	19.4
1a	2002.77	VLBA	15.0	4.74	0.18	$1.0\times(-1,1,4,16,...,1024)$	1.4×0.5,	-5.3
1b	2004.12	VLBA	15.0	3.30	0.18	$1.0\times(-1,1,4,16,...,1024)$	1.3×0.5,	-3.3

We have also collected 41 epochs VLA data of NRAO 530 at U, K and Q bands from the Sgr A* monitoring program between 2002.09 to 2003.29. The source was observed as a calibrator. The detailed information of the observations is listed in Table 1.

2.5 Data Reduction

The correlated VLBI data were calibrated and fringe-fitted using the NRAO AIPS (Astronomical Image Processing System) package. The initial amplitude calibration was made using the system temperature measurements during the observations in addition to the station gain curves.

For the VLBA polarized observations, the polarization leakage terms were determined at each epoch by using the task LPCAL in AIPS. The instrumental electric vector position angle (WVPA) was determined following the detailed procedure given by Lister et al. (2005).

The post processing of all VLBI data (EVN and VLBA observations), including editing, phase and amplitude self-calibration, and imaging was done in AIPS. The task MODELFIT in the DIFMAP package was used to fit models of the calibrated data. Elliptical and circular Gaussian brightness distribution functions were used in the model fitting.

The MERLIN data were calibrated with the D-programs (Thomasson 1986).

The VLA data were calibrated in AIPS using the standard procedure. The flux density scale was determined from the standard flux density calibrators 3C48 and 3C286.

The post-processing of the MERLIN and VLA data was carried out in AIPS and DIFMAP, including the editing, the phase and amplitude self-calibration, imaging, and model fitting.

3 RESULTS

We imaged the source using the data and carried out model fitting. Nine images at different scale were selected and shown in Figures 1 and 2 in order of decreasing resolution. The results of the model fitting are listed in Table 2. In the table column (1) gives the serial number of each figure. The rest of the columns list (2) epoch, (3) array, (4) observing band, (5) peak flux density, (6) r.m.s. (1σ), (7) contour levels and (8) restoring beam of the total intensity image, respectively.

The results of model fitting are presented in Table 3. Column (1) shows the serial number of the corresponding figure and column (2) shows the observation information, columns (3) and (4) the component name and its flux density respectively, columns (5) and (6) the radial distance and the position angle relative to the core, respectively, and columns (7), (8) and (9) the major axis, axial ratio and position angle of the major axis, respectively.

3.1 Morphology on pc Scale

The VLBA images at 15 GHz show a core-jet structure to the north in which the jet bends to north-east at a position angle about 30° to 2 mas from the core. Then, the jet bends to north-west before it returns to north-east again for about 8 mas from the core (Figs. 1 and 2a).

Polarization was detected in the core and jet components with the VLBA observations (Fig. 1). The polarized flux density and the polarization angle changed significantly near the core during the period

Table 3 The Model Fitting Results

Fig.	Obs. inf.	Comp	S (mJy)	r (mas)	PA (°)	a (mas)	b/a	PA (°)
(1)	(2)	(3)	(4)	(5)	(6)	(7)	(8)	(9)
	2000.03	Core	1,900	0.0	0.0	0.29	0.26	1.8
	VLBA	B2	308	1.04	31.7	1.04	0.08	17.0
	15 GHz	B1	323	1.84	4.1	0.72	0.28	80.0
		D1b	57.3	4.77	4.2	2.26	0.1	−45.8
		D1a	133	6.12	15.4	2.20	0.59	−52.7
		E	82.8	23.9	2.6	8.74	0.47	37.2
	Errors		6%	7%	3	7%		3
Fig. 1a	2002.77	Core	4,738	0.0	0.0	0.18	0.20	5.4
Fig. 2a	VLBA	B3	125	0.51	28.5	0.72	0.43	22.2
	15 GHz	B2	344	1.85	30.4	0.82	0.57	28.7
		B1	214	2.45	5.7	0.92	0.88	−28.7
		D1b	147	5.74	10.5	2.61	0.87	34.6
		D1a	89.0	7.91	16.1	1.48	0.30	−81.1
		E	140	23.5	0.7	6.08	0.53	46.0
	Errors		6%	7%	3	7%		3
Fig. 1b	2004.12	Core	3,468	0.0	0.0	0.31	0.20	8.0
	VLBA	B3	154	1.09	23.7	1.54	0.11	4.3
	15 GHz	B2	183	2.21	30.2	0.98	0.51	−3.3
		B1	136	2.93	3.0	2.58	0.39	16.0
		D1b	91.3	6.74	11.0	2.30	0.75	55.1
		D1a	86.0	8.23	17.0	1.19	0.46	−69.6
		E	85.9	23.6	0.8	4.64	0.30	73.0
	Errors		6%	7%	3	7%		3
Fig. 2b	1999.13	Core	2,770	0.0	0.0	1.67	1.0	157.1
	EVN	D1b	517	4.16	13.4	2.00	1.0	−168.1
	5 GHz	D0	47.8	6.64	−23.7	1.29	1.0	−144.9
		E2	378	22.6	0.8	10.0	0.35	23.6
		E1	101	29.8	−9.5	10.3	1.0	174.5
	Errors		10%	10%	5	10%		5
Fig. 2c	1999.45	Core	3,085	0.0	0.0	3.23	0.85	3.7
	VLBA	B1	1,106	3.97	13.1	6.25	0.77	−26.0
	1.6 GHz	E2	1,095	21.5	1.59	12.5	0.44	15.7
		E1	153	28.5	−11.1	5.76	1.0	−16.9
	Errors		6%	7%	3	7%		3
	1999.13	Core	4543	0.0	0.0	15.4	0.26	−5.59
	MERLIN	C2	33.3	86	−10.8	195	0.01	26.1
	5 GHz	C1	10.0	657	−41.5	371.0	0.16	−26.5
		C'1	10.0	203	88.5	249.1	0.12	16.5
		WL	56.3	11,233	−86.3	731.8	0.45	54.7
	Errors		8%	9%	3	9%		3
Fig. 2d	1998.32	Core	5031	0.0	0.0	8.4	0.63	46.7
	MERLIN	C1	16.1	709	−47.0	574.0	0.20	−40.6
	1.6 GHz	WL	151	11,158	−86.3	754.1	0.62	61.8
	Errors		8%	9%	3	9%		3
	1992.91	Core	5579	0.0	0.0	15.3	0.21	−3.3
	VLA-B	C1	10.6	611	−39.7	501.3	0.23	−57.2
	8.5 GHz	WL	45.3	11,164	−86.3	684.0	0.70	66.6
	Errors		5%	6%	3	6%		3
Fig. 2e	2003.46	Core	4381	0.0	0.0	21.9	0.20	−35.5
	VLA-A	C1	15.5	687	−38.6	536.7	0.20	−66.9
	5 GHz	WL	68.8	11,175	−86.3	723.2	0.68	59.7
		EL	38.6	12,117	74.8	8013	0.57	−20.0
	Errors		6%	6%	3	6%		3
Fig. 4f		Core	5450	0.0	0.0	27.7	1	0
	VLA-CnD	WL	29.2	11011	−86.2	1047	1	0
	15 GHz	EL	14.4	11299	72.6	6151	1	0
	Errors		6%	6%	3	6%		3
Fig. 2g	2003.29	Core	5207	0.0	0.0	162.4	0.58	15.5
	VLA-D	WL	34.2	11,100	−85.9	3697	0.36	35.4
	15 GHz	EL	12.4	12,000	72.3	6487	0.45	−40.1
	Errors		6%	7%	3	7%		3

Table 3 – *Continued.*

Fig.	Obs. inf.	Comp	S (mJy)	r (mas)	PA (°)	a (mas)	b/a	PA (°)
(1)	(2)	(3)	(4)	(5)	(6)	(7)	(8)	(9)
Fig. 2g	2002.09	Core	5075	0.0	0.0	13.3	0.20	−1.7
	VLA-A U	WL	22.1	11,200	−86.3	665.1	0.48	35.4
	Errors		6%	6%	6	6%		3
	VLA-A K	Core	5333	0.0	0.0	10.6	0.26	4.2
		WL	17.4	11,100	−86.7	632.2	0.19	−69.4
	Errors		6%	6%	3	6%		3
	VLA-A Q	Core	6273	0.0	0.0	7.2	0.24	6.0
	Errors		9%	9%	3	9%		3
	2002.38	Core	5772	0.0	0.0	21.8	0.42	55.1
	VLA-AnB U	WL	27.0	11,200	−86.5	910.8	0.55	45.8
	Errors		6%	6%	3	6%		3
	VLA-AnB K	Core	6896	0.0	0.0	16.2	0.47	52.1
		WL	17.2	11,000	−86.5	1020	0.22	63.1
	Errors		6%	6%	3	6%		3
	VLA-AnB Q	Core	5862	0.0	0.0	8.8	0.60	66.0
	Errors		9%	9%	3	9%		3
	2002.49	Core	6114	0.0	0.0	20.3	0.50	10.1
	VLA-B U	WL	32.2	11,100	−86.4	933.1	0.71	58.1
	Errors		6%	6%	3	6%		3
	VLA-B K	Core	5873	0.0	0.0	8.4	1	−6.5
		WL	11.4	11,100	−85.8	524.9	0.46	−20.8
	Errors		6%	6%	3	6%		3
	VLA-B Q	Core	7008	0.0	0.0	3.2	1	−3.0
	Errors		9%	9%	3	9%		3
	2002.75	Core	6381	0.0	0.0	32.4	0.24	63.9
	VLA-BnC U	WL	26.4	11,200	−86.5	702.3	0.77	55.3
	Errors		6%	6%	3	6%		3
	VLA-BnC K	Core	6002	0.0	0.0	46.9	0.28	86.2
		WL	20.1	10,800	−86.4	1355	1	18.4
	Errors		6%	6%	3	6%		3
	VLA-BnC Q	Core	5076	0.0	0.0	5.5	1	0
	Errors		9%	9%	3	9%		3
	2002.88	Core	5822	0.0	0.0	47.8	0.39	−42.0
	VLA-C U	WL	26.5	11,174	−86.1	910.3	0.62	−78.1
		EL	4.4	12,400	90.0	1060	1	13.2
	Errors		6%	6%	3	6%		3
	VLA-C K	Core	5890	0.0	0.0	61.8	0.25	−40.7
		WL	16.2	11,000	−86.5	478.6	1	2.7
	Errors		6%	6%	3	6%		3
	VLA-C Q	Core	4973	0.0	0.0	14.7	0.59	64.5
	Errors		9%	9%	3	9%		3
	2003.03	Core	5450	0.0	0.0	16.1	1	0
	VLA-CnD U	WL	27.2	11,100	−86.4	848.2	1	0
		EL	14.9	11,100	74.5	6401	1	0
	Errors		6%	6%	3	6%		3
	VLA-CnD K	Core	5394	0.0	0.0	9.2	1	0
		WL	13.8	11,163	−86.2	178.8	1	0
	Errors		6%	6%	3	6%		3
	VLA-CnD Q	Core	4353	0.0	0.0	16.3	1	0
		WL	8.2	11,400	−85.0	715.9	1	0
	Errors		9%	9%	3	9%		3
	2003.12	Core	5552	0.0	0.0	80.3	1	0
	VLA-D U	WL	28.2	11,200	−87.0	1438	1	0
		EL	13.8	11,000	74.9	6300	1	0
	Errors		6%	6%	3	6%		
	VLA-D K	Core	5388	0.0	0.0	40.0	1	0
		WL	19.0	11,000	−85.6	1033	1	0
		EL	7.9	10,500	63.4	5022	1	0
	Errors		6%	6%	3	6%		
	VLA-D Q	Core	4826	0.0	0.0	18.8	1	0
		WL	27.2	11,700	−85.6	2824	1	0
		EL	8.8	12,600	63.4	2886	1	0
	Errors		9%	9%	3	9%		

2002.77 – 2004.12. The polarized flux density is 6.0±0.6 mJy beam $^{-1}$ with polarization angle -22.2° at epoch 2002.77, and is 20.0±2 mJy beam $^{-1}$ at angle 59.9° at epoch 2004.12. It is clear that the polarized flux density and the polarized angle changed rapidly around the core region while they did not change significantly in the jet region.

A weak emission was detected at about 23 mas north of the core. The 15 GHz VLBA image at the epoch of 2002.77 is presented in Figure 2a.

Of the high resolution observed data (Jorstad et al. 2001), the 15 GHz VLBA data could be fitted with seven components, labelled core, B3, B2, B1, D1b, D1a and E by Jostad et al. (2001). The components, core, B1, B2 and D1 (D1a and D1b) were detected by Jostad et al. at 22 or 43 GHz with VLBA. A new component (labelled B3) was detected at epochs 2002.77 and 2004.12. The component located at about 23 mas north of the core is the one labelled E.

The EVN image shows an unbroken, wavy trajectory to the north for about 30 mas (Fig. 2b). The jet initially moves to the north-west along PA 13° for $\sim$ 5 mas from the core; it then turns abruptly to the west and then bends to the north-east in the direction almost parallel to the initial 5 mas jet. Lastly, the jet seems to turn to the west once more.

The model fitting to the EVN data shows that D1 (most of it is D1b) was detected. Another component located at 664 mas from the core at PA= -23° is also shown in the fitting. It seems that this component was ejected before D1. Thus, we labelled it D0. Component E can be fitted with two components: E1 and E2 (see Table 3).

The 1.6-GHz VLBA image exhibits a continuous jet to the north for about 40 mas. No counter jet was detected in the south at a level of 1σ $\sim$0.81 mJy beam $^{-1}$. The calibrated data can be fitted with four components, Core, B1, E1 and E2 (see Table 3).

The outburst in flux density in 2002 appeared to be associated with a new component ejected during that period. The variation of polarization may be related to the outburst, i.e., the ejection of a new jet component near the core.

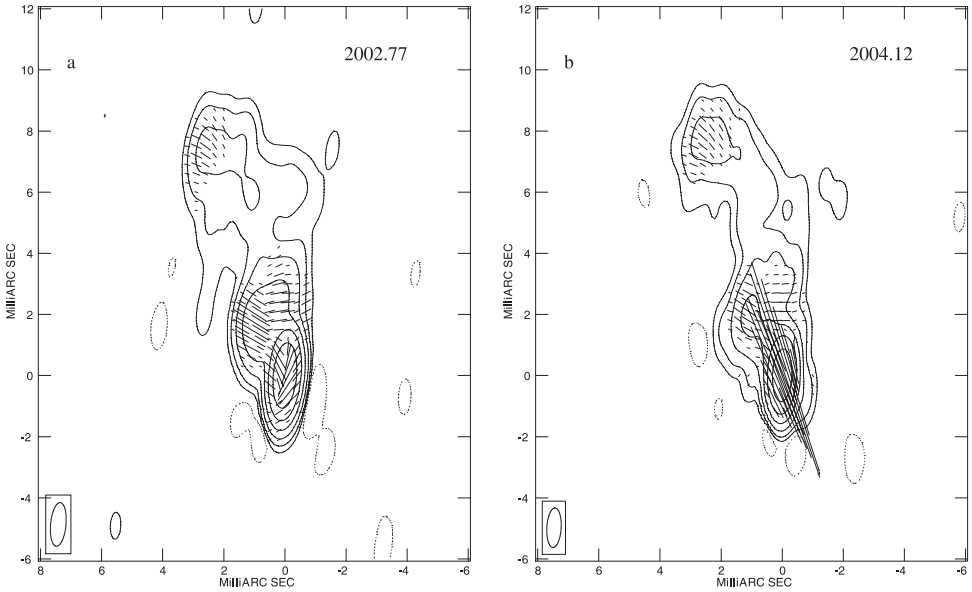

Fig. 1 VLBA images at 15 GHz in total intensity contours, the superposed sticks showing the orientation of the electric vector, a) epoch 2002.77 and b) epoch 2004.12. The contours start at 1.0 mJy beam^{-1}, and increase by a factor of 3 at each step. Polarization line 1 mas =15 mJy beam^{-1}. The peak polarization flux densities are 6.0 and 20.0 mJy beam^{-1}, respectively.

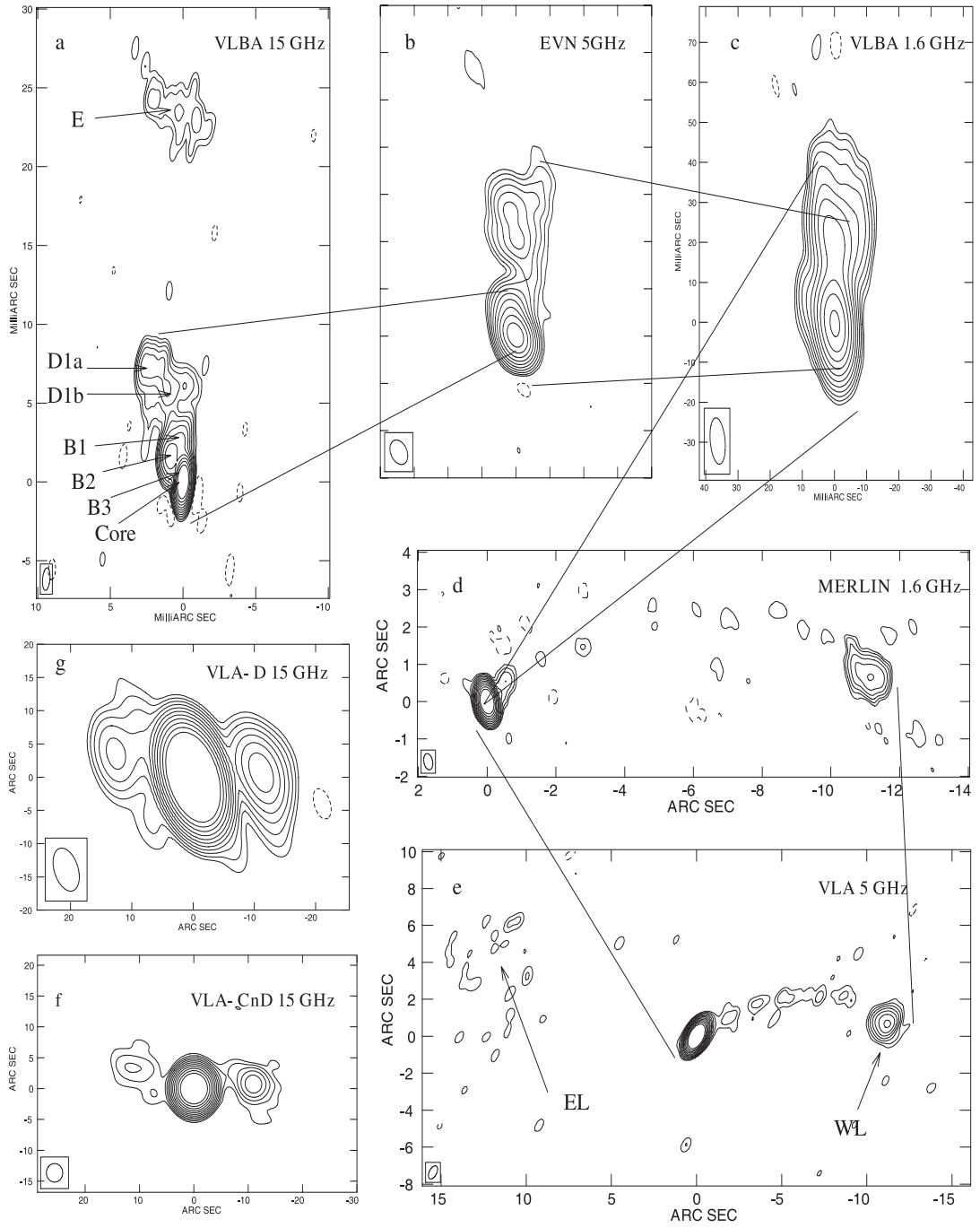

Fig. 2 Structure of NRAO 530 from pc- to kpc-scale. a) VLBA image at 15 GHz at epoch 2002.77, b) EVN image at 5 GHz, c) VLBA image at 1.6 GHz, d) MERLIN image at 1.6 GHz, e) VLA-A image at 5 GHz, f) VLA CnD image at 15 GHz, and g) VLA-D image at 15 GHz. The lowest contours are 1.0, 5.0, 2.5, 1.0, 0.4, 0.8 and 0.25 mJy beam^{-1}, respectively. Contour levels increase by a factor of 2.

3.2 Morphology on kpc Scale

The 5 GHz MERLIN image shows a core-jet structure at PA$\sim -50^\circ$ on the scale of about $1''$ and a distant component located at about $11''$ west of the core, which is labelled west Lobe (WL) in PA$\sim -86^\circ$. No clear connection between the core and the distant western component was detected in the 5 GHz MERLIN observation (see Table 3).

To obtain the extended emission of the source, we tapered down the 5-GHz MERLIN visibility data in the uv range longer than 1 mega-wavelengths with a comparable resolution of the MERLIN at 1.6 GHz. The 1.6-GHz MERLIN image presents a similar morphology to the 5 GHz MERLIN image but the arch-shaped emission connecting the core and WL is resolved. The significance of the clumpy emission in the arch structure is greater than 3σ. We can rule out the possibility of it being an artefact sidelobe because the dirty beam pattern of the point spread function had been removed in the cleaning process. The core-jet structure and the west component are clearly detected (see Fig. 2d and Table 3). The weak connecting emission looks like a ballistic trajectory. This indicates that the west component is a lobe or a hotspot of NRAO 530.

The VLA image at 8.4-GHz shows a similar structure to that of MERLIN, and confirms the detection of the low brightness emission at 3σ significance between the core and the component WL. It suggests that the emitting material in WL is powered by the central engine.

A stronger emission between the core and WL is shown in the VLA image at 5 GHz (Fig. 2e) at a significance of 5σ. A patch of weak diffuse emission is detected in the region about $12.5''$ east (PA=70°) of the core, which appears to be the counter lobe of the source (Fig. 2f). The east and west components were detected at a significance of 5σ and 20σ, respectively The ratio of flux density between the two components is about 2.5:1. This ratio suggests that the relativistic effect may still play a role in the larger scale jets. No clear connection between the east component and the core was detected down to the limit of 0.15 mJy beam^{-1}.

The image (Fig. 2f) of VLA observation with CnD array at 15 GHz shows an "S" shaped morphology. The west jets bend into the west lobe in the north-west direction while the east jets bend into the east lobe in the south-east direction.

The lowest resolution of the VLA image is presented in Figure 2g. The morphology shown in the large scale is consistent with a symmetrical double-lobe source.

3.3 Spectral Index on kpc Scale

NRAO 530 was imaged using the 41-epoch VLA data at U, K and Q bands from 2002.09 to 2003.29 with a tapper function to weight down the long baseline visibility points in order to unify angular resolution of $1''$ for the data of the three bands observed in all the configurations. The detection of core, east and west lobes is detailed in Table 4. The flux densities of the core at 15 and 22 GHz are plotted in Figure 3. It is clear that there were two outbursts during 2002. The peaks are located around epochs 2002.30 and 2002.60, respectively. It is generally believed that the outbursts correspond to shocked jet ejections in the nucleus (e.g., Valtaoja et al. 1999).

The simultaneous VLA observations at U and K bands allow us to estimate the spectral indices of the components on kpc scale. The spectral indices of the core and the lobes are plotted in Figure 4. It is clear that the core has a flat spectrum ($\alpha < 0.5$, $S \propto \nu^{-\alpha}$), while the lobes have steep spectra ($\alpha \sim 0.5 - 2.5$). The spectral index difference between the core and lobe is consistent with the fact that the core component is optically thick and the lobe relatively thin. The arch-like structure is the track through which high energy particles are transported from the central engine to the lobe. The particles are re-accelerated through shocks in the lobes.

3.4 Superluminal Motion of the Jet Components

The results from model fitting of the calibrated data are listed in Table 3. Our results confirm the suggestion of Jorstad et al. (2001) that the south component is the core and the jet is ejected to the north. A new component is detected at 15 GHz at epochs 2002.77 and 2004.12.

Proper motions of the jet components of QSO NRAO 530 have been reported by Bower et al. (1997), Jorstad et al. (2001) and Feng et al. (2006). With a suitable time sampling of the VLBI data from this paper and the previous literature (see Table 5), we plot the position of the components D1a, D1b, B1, B2 and B3

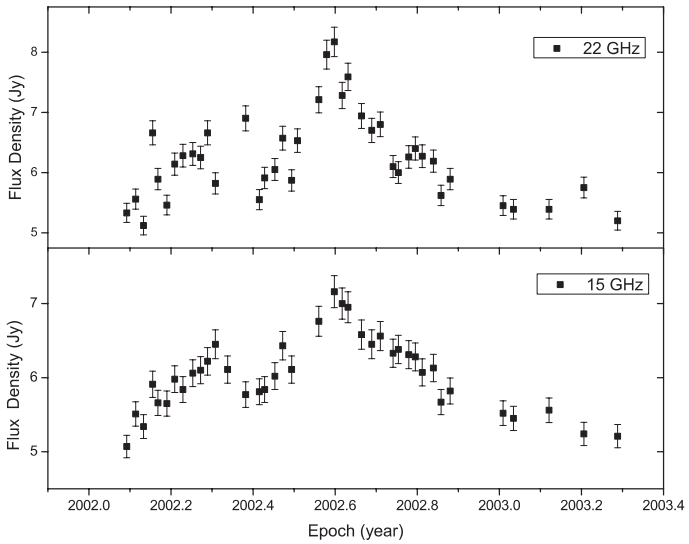

Fig. 3 Flux densities of the core component of NRAO 530 at 22 and 15 GHz observed with VLA. The error bars are 1σ error bars.

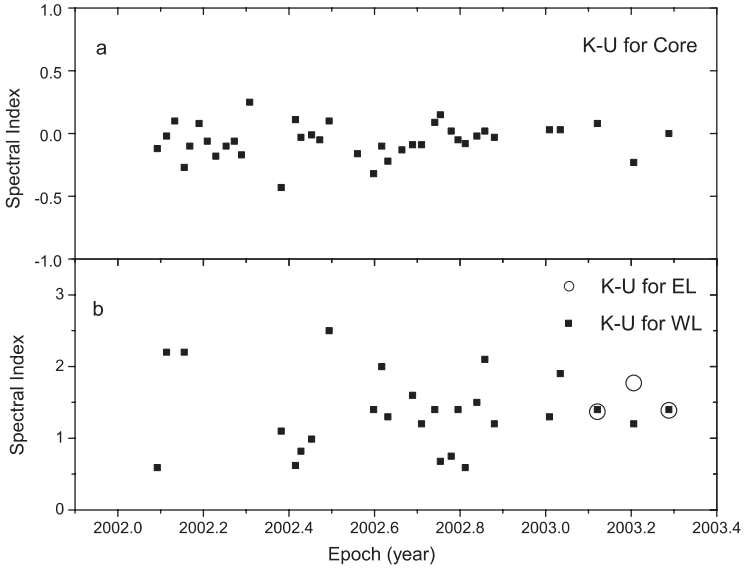

Fig. 4 Spectral indices of the core and the lobes of NRAO 530 from VLA observations. The 1σ error for the spectral indices is estimated to be 0.2.

with respect to the core in Figure 5. The apparent velocities of the jet components are calculated and listed in Table 6.

Our results confirm the superluminal motion of the jet components D1 (D1a & D1b), B1 and B2. The jet components kept moving steadily with apparent velocities in the range of 13.6 to 25.2c. The results from the 15 GHz VLBA observations at the epochs of 2002 and 2004, the component B3 could be associated with the radio outburst peaked at epoch 2002.30. We estimated its proper motion to be 0.43 mas yr $^{-1}$ by using the two epoch data points. Note that Feng et al. (2006) found a jet component in NRAO 530, labelled

Table 4 The Detection of Lobes with the VLA Monitoring Data

Array	U Band			K band			Q band		
	C	W	E	C	W	E	C	W	E
A	√	√		√	√		√		
AnB	√	√		√	√		√		
B	√	√		√	√		√		
BnC	√	√		√	√		√		
C	√	√	√	√	√		√		
CnD	√	√	√	√	√		√	√	
D	√	√	√	√	√	√	√	√	√

Note: C – Core, W – West lobe, E – East lobe

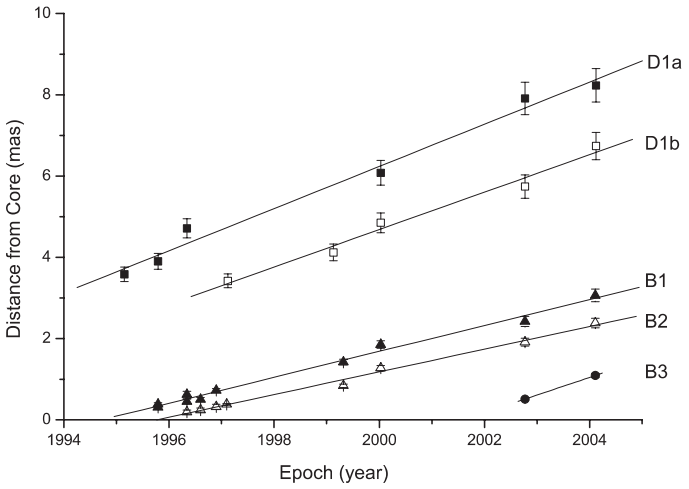

Fig. 5 Proper motions of the jet components D1a, D1b, B1, B2 and B3 of NRAO 530. The filled squares show the position of D1a from the core. The empty squares, filled triangles, empty triangle and filled circles show the positions from the core of the components D1b, B1, B2 and B3, respectively.

F, at 0.22 mas from the core with a flux density of 0.34 Jy on 1999.32 at 43.1 GHz. We can not exclude the possibility that our B3 and F were the same component. If this is the case, the apparent speed of B3 will be much slower (about 0.13 mas yr^{-1}). More observations are needed to confirm the superluminal motion of the new component.

3.5 Doppler Factors and Viewing Angles

Doppler boosting happens frequently in the relativistic jets of quasars. To obtain more details about the emission mechanism in the jet of NRAO 530, we estimated the Doppler factors by two independent approaches: (1) inverse Compton Doppler factors $\delta_{\rm IC}$ and (2) equipartition Doppler factors $\delta_{\rm eq}$. For the former, we assume that all the X-ray flux density is produced from the synchrotron radio photons through inverse Compton scattering process (e.g. Güijosa & Daly 1996). Thus,

$$\delta_{\rm IC} = f(\alpha) S_m (1+z) \Big[\frac{\ln(\nu_b/\nu_{\rm op}\nu_{\rm x}^{-\alpha})}{S_{\rm x}\theta_d^{6+4\alpha}\nu_{\rm op}^{5+3\alpha}} \Big]^{1/(4+2\alpha)}, \quad (1)$$

where $S_{\rm x}$ is the observed X-ray flux density in Jy at frequency $\nu_{\rm x}$ in keV, ν_b the synchrotron high-frequency cutoff (assumed to be 10^5 GHz), $\nu_{\rm op}$ the observed frequency in GHz, $S_{\rm op}$ the flux density in Jy at $\nu_{\rm op}$, θ_d the angular diameter of a homogenous sphere in mas, and we take $\theta_d = 1.8\,\theta_{\rm FWHM}$ (in case of elliptical Gaussians, $\theta_{\rm FWHM}$=$\sqrt{\theta_1\theta_2}$) to correct the observed angular diameter $\theta_{\rm FWHM}$ (Marscher 1977, 1987).

Table 5 VLBI Data Used for the Proper Motion Estimation

Epoch	Freq. (GHz)	Component Label	Reference
1995.15	22.2	D1a	a
1995.79	22.2	D1a	a
	43.2	B1	a
1996.34	22.2	D1a, B1	a
	43.2	B1, B2	a
1996.60	43.2	B1, B2	a
1996.90	43.2	B1, B2	a
1997.12	15.4	D1b, B2	b
1999.13	5.0	D1b	c
1999.32	43.1	B1, B2	b
2000.03	15.3	D1a, D1b, B1, B2	c
2002.77	15.3	D1a, D1b, B1, B2, B3	c
2004.11	15.3	D1a, D1b, B1, B2, B3	c

Notes: a – Jorstad et al. (2001); b – Feng et al. (2006); c – this paper.

Table 6 Proper Motion of the Jet Components

No.	Component Label	Proper Motion (mas year^{-1})	Apparent Speed (c)
1	D1a	0.52 ± 0.03	25.2 ± 1.4
2	D1b	0.46 ± 0.04	22.3 ± 1.9
3	B1	0.32 ± 0.01	15.5 ± 0.5
4	B2	0.28 ± 0.01	13.6 ± 0.5
5	B3	0.43 ± 0.08	20.8 ± 3.9

Notes: Errors are obtained by making use of the position errors of B3 in Table 3.

While α is defined as in $S_\nu \propto \nu^{-\alpha}$, $f(\alpha) \approx 0.08\,\alpha + 0.14$. The flux density S_m is the value which would be obtained at $\nu_{\rm op}$ by extrapolating the optically thin spectrum (Marscher 1977, 1987). For $\alpha = 0.75$, it is about a factor of 2, which is larger than the observed peak flux density $S_{\rm op}$ (Marscher 1977), here we take 2 in our calculations. The X-ray flux density is 0.2 μJy at 1 keV for NRAO 530 (Ghisellini et al. 1993).

From the assumption of equipartition between the energy of radiating particles and the magnetic field (e.g. Güijosa & Daly 1996), we have

$$\delta_{\rm eq} = [[10^3 F(\alpha)]^{34}\{[1-(1+z)^{-1/2}]/(2h)\}^{-2} S_{\rm op}^{16}\theta_d^{-34} \times(1+z)^{15+2\alpha}(\nu_{\rm op}\times 10^3)^{(2\alpha-35)}]^{1/(13+2\alpha)}, \quad (2)$$

where z is the redshift, $\nu_{\rm op}$, $S_{\rm op}$, θ_d and α are same as in Equation (1). We assume the observed frequency is at the radio peak since the dominant core component at the frequency of observation should be near its peak, and α is taken to be 0.75 as the optical thin spectral index. In this case $F(0.75)$= 3.4 (Scott & Read 1977).

Based on Equations (1) and (2), $\delta_{\rm IC}$ and $\delta_{\rm eq}$ are estimated and listed in Table 7 for the three epochs of the VLBA data at 15 GHz. The estimated $\delta_{\rm IC}$ and $\delta_{\rm eq}$ of the VLBI core are comparable. It is clear that the core has a much stronger Doppler boosting during the outburst at epoch 2002.77. In the quiescent state, our value of 4.8 is consistent with 5.2 estimated by Güijosa & Daly (1996).

The observed brightness temperature $T_b^{'}$ of a Gaussian component is given by Güijosa & Daly (1996),

$$T_b^{'}({\rm K}) = 1.77\times 10^{12}\frac{S_{\rm op}}{\theta_d^2\nu_{\rm op}^2}, \quad (3)$$

where $S_{\rm op}$, θ_d, and $\nu_{\rm op}$ are the same as in Equation (2).

With the $T_b^{'}$ and $\delta_{\rm eq}$ values in Table 7, the intrinsic brightness temperature $T_r = T_b(1+z)/\delta$ (Güijosa & Daly 1996) can be estimated (see Table 7). The value of T_r derived from our data is below the equipartition brightness temperature limit $\sim 10^{11}$ K.

Table 7 Doppler Factor and Brightness Temperature of the VLBI Core

Obs.	$\nu_{\rm obs}$ (GHz)	$S_{\rm obs}$ (Jy)	$\theta_{\rm FWHM}$ (mas)	$\delta_{\rm IC}$	$\delta_{\rm eq}$	$T_b^{'}$ (10^{12} K)	T_r (10^{12}K)
(1)	(2)	(3)	(4)	(5)	(6)	(7)	(8)
2000.03	15.37	1.9	0.15	8.4	4.8	0.2	0.07
2002.77	15.37	4.7	0.08	56.4	54.1	1.7	0.05
2004.12	15.37	3.5	0.14	17.3	10.9	0.4	0.07

Notes: Col. (1) epoch, col. (2) frequency of VLBI observation, col. (3) VLBI flux density, col. (4) FWHM size of VLBI core, col. (5) inverse Compton Doppler factor, col. (6) equipartition Doppler factor, col. (7) observed source brightness temperature, and col. (8) brightness temperature in the rest frames of sources for the equipartition model of homogenous sphere source.

A well-known relation between the apparent speed $\beta_{\rm app}$ and the peculiar velocity relative to the Hubble flow β of the source is (Rees & Simon 1968; Blandford et al. 1977),

$$\beta_{\rm app} = \frac{\beta \sin\theta}{1 - \beta\cos\theta}, \tag{4}$$

where β is in units of light speed c, θ is the angle between the direction of motion and the line of sight in degrees. Then, the Lorentz factor $\gamma \equiv 1/\sqrt{1-\beta^2}$ and the viewing angle θ can be computed (Ghisellini et al. 1993),

$$\gamma = \frac{\beta_{\rm app}^2 + \delta^2 + 1}{2\delta}, \tag{5}$$

$$\tan\theta = \frac{2\beta_{\rm app}}{\beta_{\rm app}^2 + \delta^2 - 1}. \tag{6}$$

Assuming the jet components to have the same Doppler boosting as the core ($\delta_{\rm eq}$=4.8), we estimated the Lorentz factor for the jet components (D1a, D1b, B1, B2 and B3) with Equation (5) to be 68.7, 54.3, 27.5, 21.8 and 47.6, and their viewing angles with Equation (6) to be 4.4 °, 4.9°, 6.7°, 7.5° and 5.2°, respectively. It is obvious that the jet components moved in the direction very close to the line of sight.

4 DISCUSSION

QSO NRAO 530 has a wavy jet at pc-scale to the north of the core, while it has a double lobe at kpc-scale in the east-west direction. Since we still lack detection of emission on scales from several tens of mas (∼300 pc) to about one arcsec (∼8 kpc), the detailed process of how the jets changed from a north-south orientation on pc-scale to an east-west orientation on kpc-scale is still missing.

A statistical analysis of the position angle differences (ΔPA) between pc- and kpc-scale structures of EGRET-detected AGNs shows that γ-ray quasars are aligned with the radio jet, while γ-ray BL Lac objects have large ΔPA (Hong et al. 1998). A γ-ray BL Lac object is usually associated with a radio jet aligned with the line of sight on pc-scale. Consequently, the observed large ΔPA is believed to be a projection effect.

Let us consider how the position angle of a jet component changes with its distance from the core. In Figure 6 a series of jet components on different scales are plotted. The data include six points, B3, B2, B1, D1b, D1a and E, from VLBA at 15 GHz at epoch 2000.03, three points, C1, C2, WL, from MERLIN at 5 GHz at epoch 1999.13, and four points of the west large-scale Jets from VLA at 5 GHz at epoch 2003.46. As can be seen from Figure 6, the jets show a wavy trajectory with the position angle varying in the range 40 to –20° on the small scale. On the large scale the jets bend smoothly towards the west. The large position angle change of about 90° between the pc- and kpc-scale structures is probably due to a helical jet geometry combined with small viewing angles. In the low-pitch helical geometry, the VLBI jet follows the helical path in a direction perpendicular to the axis of the helix, while the large scale jet moves inside the original helical cone or perhaps wraps around a cylinder (Conway 1993; Hong et al. 2004). Then, generally, the observed morphology will show an arch-shaped structure from pc- to kpc-scale as observed in NRAO 530.

It is probably the case that the source is basically a two-sided jet in the north-south direction with the northern jet approaching us on a helical path and bending to the west lobe. The northern jet is easy to detect

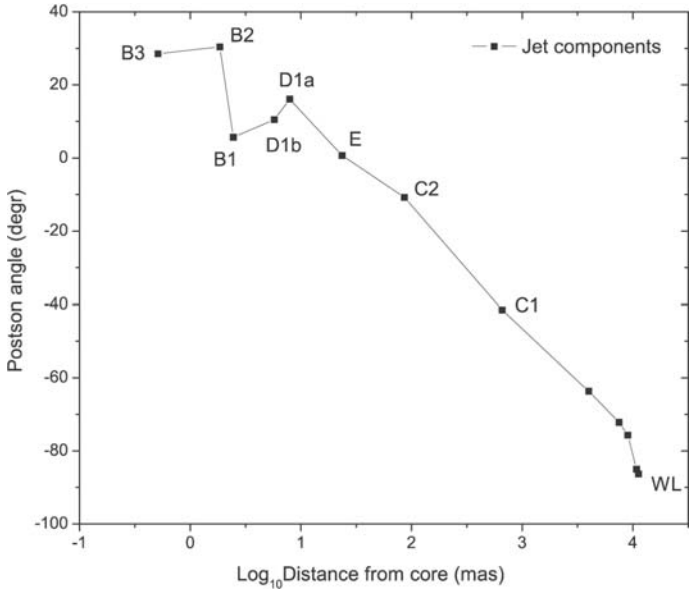

Fig. 6 Trajectory of jet components — The jets on different scales were based on data from the representative antenna arrays of VLBA, MERLIN and VLA. The vertical axis represents the position angle of the jet components relative to the core. The four unlabelled points in the lower-right corner are the components between the core and WL in the VLA 5 GHz data.

because of its high Doppler boosting. The counter jet in the south that is moving away from us and is bent towards the east lobe, was not detected in the VLBI observations due to the limited sensitivity. The large change (ΔPA=90°) in the position angle of the components in the jets of NRAO 530 could be a projection effect of the helical trajectory since the pc jets are very close to the line of the sight. This is similar to the case of EGRET-detected BL Lac objects (Hong et al. 1998).

Of course, we need to further examine alternative bending mechanisms such as bending through the interaction between the jet material and the ISM (interstellar medium) or ICM (intra-cluster medium), similar to the bending of jets in WAT (wide-angle-tail) and/or NAT (narrow-angel-tail) radio sources associated with galaxies in rich clusters (Burns 2002). In the case of bending due to ram pressure from the ICM, the lobe and counter lobe would be located in the downstream of the ICM in the frame of the QSO. However, the large scale (kpc) shape of NRAO 530 shows an 'S' shaped morphology. Such a distortion is often explained by 'precession' or wobbling of the central engine. Thus, bending by the ram pressure appears to be less favored by our observations. Disk precession or wobbling is plausibly the main process responsible for the observed radio morphology from pc to kpc scales.

5 CONCLUSIONS

5.1 On the pc Scale

Based on our observations and analysis, our conclusions are as follows:

On the scale of a few mas, the oscillating VLBI jet of NRAO 530 consists of a number of emission components north of the core. These jet components moving at relativistic velocities have apparent speeds in the range of 13.6 to 25.2c in directions very close to the line of sight and show high Doppler boosting. The counter jet was detected on pc-scale.

A new jet component was detected at 15 GHz with the VLBA observations at epochs 2002.77 and 2004.12, which may correspond to the radio outburst in 2002.

Polarization was detected in the jet components with the VLBA at 15 GHz. Its properties near the core changed rapidly, by a factor of 3 in the polarized flux density and by about $80\,^{\circ}$ in the polarization angle

between 2002 and 2004, while they are stable in the jet components. The variation in polarization can be attributed to the new jet component associated with the radio outburst in 2002.

5.2 On kpc Scale

The source exhibits a double lobe in the east-west direction. The west lobe is much stronger than the east lobe: the intensity ratio is about 2.5. A core-jet structure at the scale of half arcsecond in PA $\sim -40\,^{\circ}$ and a weak emission in the shape of an arch is clearly detected between the core and the west lobe, which means that the lobe is powered by the central engine. Moreover, the core shows a flat spectral index, while the lobes show steep spectral indices.

5.3 Connection from pc to kpc Scale

On the kpc scale, the source basically consists of a two-sided lobe in west-east with an arch structure (a curved jet) that connects the core to the west lobe. The curved kpc jet is likely associated with the northern jet detected on the pc scale. The large change in position angle might be caused by projection effect of a helical trajectory since the pc jets are very close to the line of sight. The "S" shaped morphology may rule out the possibility of ram pressure for the bending of the jets. The bending is more likely to be caused by the precession process.

Acknowledgements This research is supported by the National Natural Science Foundation of China (NSFC, Grants 10473018, 10328306 and 10333020), and the Science and Technology Commission of Shanghai Municipality (06DZ22101). The authors are grateful for the technical support by the staff of the EVN, MERLIN and VLA. The European VLBI Network is a joint facility of European, Chinese, South African and other radio astronomy institutes funded by their national research councils. MERLIN is a national facility operated by the University of Manchester at Jodrell Bank Observatory on behalf of PPARC. The VLA is a facility of the National Radio Astronomy Observatory, which is operated by the Associated Universities Inc., under a cooperative agreement with the National Science Foundation. The authors thank the MERLIN staff, Dr. S. T. Garrington, for the calibration of the MERLIN data. The authors thank M. Lister for kindly providing the VLBA data. This research has made use of the NASA/IPAC Extragalactic Database (NED).

References

Blandford R. D., McKee C. F., 1977, Nature, 267, 211
Blandford R. D., Königl A., 1979, ApJ, 232, 34
Bondi M., Padrielli L., Gregorini L. et al., 1994, A&A, 287, 390
Bower G. C., Backer D. C., Wright M. et al., 1997, ApJ, 484, 118
Brinkmann W., Siebert J., Boller Th., 1994, A&A, 281, 355
Burns J. O., Loken C., Roettiger K. et al., 2002, Stormy weather and cluster radio galaxies, New Astronomy Reviews, Volume 46, Issue 2–7, p.135
Feng S. W., Shen Z. Q., Cai H. B. et al., 2006, A&A, 456, 97
Fichtel C. E., Bertsch D. L., Chiang J. et al., 1994, ApJS, 94, 555
Güijosa A., Daly R. A., 1996, ApJ, 461, 600
Padovani P., Ghisellini G., Fabian A. C. et al., 1993, ApJ, 407, 65
Hong X. Y., Jiang D. R., Shen Z. Q., 1998, A&A, 330, 45
Hong X. Y., Venturi T., Wan T. S. et al., 1999, A&AS, 134, 201
Hong X. Y., Jiang D. R., Gurvits L. I. et al., 2004, A&A, 417, 887
Jorstad S. G., Marscher A. P., Mattox J. R. et al., 2001, ApJS, 134, 181
Junkkarinen V., 1984, PASP, 96, 539
Lister M. L., Homan D. C., 2005, AJ, 130, 1389
Marscher A. P., 1977, ApJ, 216, 244
Marscher A. P., 1987, In: Zensus J. A., Perason T. J., eds., Superluminal Radio Sources, Cambridge: Cambridge Univ. Press, 280
Perley R. A., 1982, AJ, 87, 859
Readhead A. C. S., 1994, ApJ, 426, 51

Rees M. J., Simon M., 1968, ApJ, 152, 145
Riess A. G., Strolger L. G., Tonry J. et al., 2005, ApJ, 627, 579
Riess A. G., Li W. D., Stetsen P. B. et al., 2005, ApJ, 627, 579
Romney J., Padrielli L., Bartel N. et al., 1984, A&A, 135, 289
Scott, M. A., Readhead, A. C. S., 1977, MNRAS, 180, 539
Shen Z. Q., Wan T. S., Moran J. M. et al., 1997, AJ, 114, 1999
Thomasson P., 1986, QJRAS, 27, 413
Thompson D. J., Bertsch D. L., Dingus B. L. et al., 1995, ApJS, 101, 259
Tingay S. J., Murphy D. W., Edwards P. G., 1998, ApJ, 500, 673
Valtaoja E., Lainela M., Terasranta H. et al., 1999, AJ, 120, 95
Whelch W. J., Spinrad H., 1973, PASP, 85, 456